Cosmology with AGN dust time lags–simulating the new VEILS survey

S. F. Hönig,[1][*] D. Watson,[2] M. Kishimoto,[3] P. Gandhi,[1] M. Goad,[4] K. Horne,[5] F. Shankar,[1] M. Banerji,[6,7] B. Boulderstone,[1] M. Jarvis,[8,9] M. Smith[1] and M. Sullivan[1]

[1]*Department of Physics and Astronomy, University of Southampton, Highfield Campus, Southampton SO17 1BJ, UK*
[2]*Dark Cosmology Centre, Niels Bohr Institute, University of Copenhagen, Juliane Maries Vej 30, DK-2100 Copenhagen Ø, Denmark*
[3]*Department of Physics, Faculty of Science, Kyoto Sangyo University, Kamigamo-motoyama, Kita-ku, Kyoto 603-8555, Japan*
[4]*Department of Physics and Astronomy, College of Science and Engineering, University of Leicester, University Road, Leicester LE1 7RH, UK*
[5]*SUPA Physics and Astronomy, University of St Andrews, KY16 9SS Scotland, UK*
[6]*Institute of Astronomy, University of Cambridge, Madingley Road, Cambridge CB3 0HA, UK*
[7]*Kavli Institute for Cosmology, University of Cambridge, Madingley Road, Cambridge CB3 0HA, UK*
[8]*Department of Physics, Oxford Astrophysics, University of Oxford, Keble Road, Oxford OX1 3RH, UK*
[9]*Physics Department, University of the Western Cape, Cape Town 7535, Republic of South Africa*

ABSTRACT

The time lag between optical and near-infrared continuum emission in active galactic nuclei (AGN) shows a tight correlation with luminosity and has been proposed as a standardizable candle for cosmology. In this paper, we explore the use of these AGN hot-dust time lags for cosmological model fitting under the constraints of the new VISTA Extragalactic Infrared Legacy Survey (VEILS). This new survey will target a 9 deg^2 field observed in J and K_s band with a 14-d cadence and will run for 3 yr. The same area will be covered simultaneously in the optical $griz$ bands by the Dark Energy Survey, providing complementary time-domain optical data. We perform realistic simulations of the survey setup, showing that we expect to recover dust time lags for about 450 objects out of a total of 1350 optical type 1 AGN, spanning a redshift range of $0.1 < z < 1.2$. We use the lags recovered from our simulations to calculate precise distance moduli, establish a Hubble diagram, and fit cosmological models. Assuming realistic scatter in the distribution of the dust around the AGN as well as in the normalization of the lag–luminosity relation, we are able to constrain Ω_Λ in ΛCDM with similar accuracy as current supernova samples. We discuss the benefits of combining AGN and supernovae for cosmology and connect the present work to future attempts to reach out to redshifts of $z > 4$.

Key words: galaxies: active – distance scale – infrared: galaxies.

1 INTRODUCTION

Arguably 10 per cent of all large galaxies host an active galactic nucleus (AGN) in their centre. Given their high luminosities, AGN can be detected from low-redshift out to the early universe at $z > 7$. Moreover, on human timescales, AGN are rather predictable with only a few sources turning on or off completely (e.g. Keel et al. 2012a,b). These traits would make them desirable tools for cosmology if their emission were standardizable.

Several routes are currently being pursued to establish AGN as standard candles. Watson et al. (2011) showed that the known relation between the size of the broad emission line region and AGN luminosity can be used to constrain cosmological parameters (see also Haas et al. 2011; Czerny et al. 2013; King et al. 2014). The sizes

of these structures are determined using the time lags between the incident radiation and the reaction in the reprocessed emission from the observed region. Alternatively to emission lines, the lag between the optical continuum and the dust continuum correlates with luminosity and can also serve as a standard candle (e.g. Oknyanskij et al. 1999; Oknyanskij & Horne 2001; Hönig 2014; Yoshii et al. 2014). Beyond this, it was proposed to use either the emission line time lags (in combination with interferometry; Elvis & Karovska 2002), lag profiles (based on photoionization modelling; Horne, Korista & Goad 2003) or the dust lags (with infrared interferometry; Hönig et al. 2014, demonstrated for NGC 4151) as standard rulers, which set an absolute distance scale to AGN and directly measure the Hubble constant H_0.

The major advantages of dust time lags as compared to emission line lags are (1) their tighter relation between lag and luminosity, when considering the same set of objects (e.g. Koshida et al. 2014), and (2) the use of photometry instead of spectroscopy. On the other

*E-mail: s.hoenig@soton.ac.uk

hand, broad emission line lags can be measured out to redshift 4 or even beyond (e.g. Watson et al. 2011; Czerny et al. 2013; King et al. 2014, 2015). When combined, both AGN-standardized candles will explore a large region in redshift space.

In this paper, we provide the scientific motivation, foundation, and simulations for using AGN hot-dust time lags as a standard candle in the redshift range $0.1 < z < 1.2$. This range is motivated by the fact that ground-based facilities with $\sim 2\,\mu m$ imaging capability can be used for a systematic survey. We focus on the design of the VISTA Extragalactic Infrared Legacy Survey (VEILS), a new European Southern Observatory (ESO) public survey scheduled to run on the 4-m VISTA telescope for 3 yr starting 2017. In the next section, we will briefly review the physical background of the size–luminosity relation in the near-infrared (IR) and discuss some characteristics as constrained by observations. In Section 3, we will derive the equations to turn lags into distance moduli, which are required to establish a Hubble diagram and fit cosmological models. In Section 4, we present our simulations of VEILS AGN light curves and discuss the methods employed to recover time lags. In Section 5, we show the results of our simulations and quantify the constraints on cosmological parameters we can expect from the survey, together with a comparison to type Ia supernovae. Practical challenges and strategies are outlined in Section 6. Finally, we summarize our findings and present the broader context and legacy of the VEILS AGN variability survey in Section 7.

2 THE LAG–LUMINOSITY RELATION IN THE NEAR-IR

The multiwavelength emission of AGN shows a prominent IR bump starting at about $1\,\mu m$ and extending to 100–$1000\,\mu m$ with a peak in the 20–$30\,\mu m$ range.[1] This emission is associated with thermal reprocessing of the ultraviolet (UV) and optical radiation from the 'big blue bump' (BBB; or accretion disc) much closer to the black hole (dust-to-BBB size ratio $\gtrsim 20$).

Dust can only survive temperatures up to about $T_{sub} \sim 1500$ K, above which the grains sublimate. This implies that the near-IR emission at 1–$2\,\mu m$ delineates a sharp boundary between dust-free and dust-containing gas, with its exact size set by the (solid-state) properties of the dust grains (chemical composition, size; e.g. Barvainis 1987; Phinney 1989). Thus, using the radiative transfer equations in thermal equilibrium, we can relate the AGN luminosity L_{AGN} to the hot-dust emission close to the sublimation radius r_{sub} as (Hönig & Kishimoto 2011)

$$L_{AGN} = 16\pi r_{sub}^2 f_{abs}^{-1} Q_{abs;P}(T_{sub})\, \sigma_{SB} T_{sub}^4, \tag{1}$$

where f_{abs} is the fraction of incident AGN flux absorbed per dust particle, σ_{SB} is the Stefan–Boltzmann constant, and $Q_{abs;P}(T_{sub})$ is the normalized Planck-mean absorption efficiency of the dust for given sublimation temperature T_{sub}, i.e. $Q_{abs;P}(T_{sub}) = \int Q_{abs;\nu}\pi B_\nu(T_{sub})\mathrm{d}\nu/(\sigma_{SB}T_{sub}^4)$. Most importantly, f_{abs} and $Q_{abs;P}$ are both parameters approaching unity for large dust grains, which emit very similarly to a blackbody.

We can now simplify this equation by absorbing all constant parameters (including T_{sub}, $Q_{abs;P}$, and f_{abs}) into a normalization

---

[1] Note that in many AGN-hosting galaxies, the IR emission peaks at much longer wavelengths. These peaks are associated with star formation in the host galaxy or nuclear region rather than the AGN itself. While the star formation contamination might be an issue in the mid- and far-IR, it does not affect the near-IR emission, in particular the variable component seen from the AGN.

parameter k_n. After replacing r_{sub} with the corresponding time lag $\tau_{sub} = r_{sub}/c$, we obtain

$$L_{AGN} = k_n \cdot \tau_{sub}^2. \tag{2}$$

In this notation, the actual object-to-object differences in hot-dust composition, geometry, and global distribution are reflected by the observed scatter σ_k in the normalization of the lag–luminosity relation of an AGN sample. Interestingly, this scatter is not very large. When using the V band as a proxy for L_{AGN} and observing lags between the V and K bands, Koshida et al. (2014) find $\log \sigma_k = 0.14$–0.16 dex (see their table 9), which implies similar overall characteristics of the hot-dust emitting region in their sample of 17 AGN (see also Appendix A). These similarities can be easily understood: first, when observing at wavelengths equivalent to temperatures of 1500 K or higher, the emission is restricted to grains that can actually survive such high temperatures. Indeed, silicate dust grains already sublimate at lower temperatures of 800–1200 K while carbonaceous grains can get hotter (e.g. Phinney 1989). Secondly, when observing fluxes from a relatively confined region, the emission will be biased towards grains with higher emissivity (= closer to blackbody radiation), which are typically the larger grains within the composition. Therefore, the emission at wavelengths close to the (carbonaceous) sublimation temperature will be dominated by blackbody-like dust grains (large, carbon) regardless of the details of the original ISM composition. This is strongly supported by surface emissivity measurements of nearby AGN in the K band using IR interferometry (Kishimoto et al. 2011b).

3 USING DUST TIME LAGS AS STANDARD CANDLES

Both the observational evidence and the rather simple radiation and solid-state physics at work underline the promise of using the hot-dust lag–luminosity relation for cosmological applications. For this, we have to turn the theoretical framework outlined in the previous section into an observational tool. The common function to test the standard model in cosmology is the relation between distance and redshift. Given the lag–luminosity relation, we need to determine the luminosity distance $D_L = (1 + z) \cdot c/H_0 \int \mathrm{d}z/E(z)$ of an AGN and compare it to its measured redshift z. Here, H_0 is the Hubble constant and $E(z) = (\Omega_m(1 + z)^3 + \Omega_\Lambda(1 + z)^{3(1+w)})^{1/2}$ [assuming a $w\Lambda$ cold dark matter (wCDM) cosmological model without curvature]. D_L is related to the distance modulus $m - M = 5\log D_L/10\,\mathrm{pc}$ with the absolute magnitude M to be determined from the lag–luminosity relation.

The lag–luminosity relation as written in equation (2) determines the bolometric AGN luminosity from the lag. In practice, it is difficult to measure the full SED of the AGN that contributes to dust heating. However, observations have shown that replacing the total luminosity with a monochromatic proxy in the rest-frame optical waveband regime provides small-enough scatter (e.g. Suganuma et al. 2006; Kishimoto et al. 2007; Koshida et al. 2014, see also previous section). We will follow the established convention and use the rest-frame V-band magnitude at 550 nm as the proxy for L_{AGN} and measure the K_s band to determine the hot-dust time lag. Therefore, the standard candle relation for the hot-dust radius of AGN can be written as

$$m_V - M_V^* = m_V + 2.5\log k_n + 5\log \frac{\tau_K}{1 + z}, \tag{3}$$

where m_V is the rest-frame 550 nm apparent magnitude and the factor $(1 + z)^{-1}$ accounts for the relativistic time dilation of the lags.

In this prescription, k_n implicitly absorbs both the normalization of the lag–luminosity relation as well as H_0 since they are essentially indistinguishable for practical purposes. k_n has to be determined either from a low-redshift sample that does not distinguish between different cosmological models or by a global fit to a large sample. Since k_n absorbs the absolute normalization of the size–luminosity relation, M_V^* should not be considered as the true absolute magnitude but rather a close proxy for M_V, which is a common aspect of standardizable candles (e.g. supernovae).

We mention that there have been attempts to estimate H_0 from the normalization of the AGN Hubble diagram using dust time lags (Yoshii et al. 2014). In practice, this is rather difficult since it requires interpreting the normalization of the lag–luminosity relation as a result of the dust grain emissivity at the sublimation radius. This involves using redshift-based luminosity distances to convert AGN flux to luminosity, thereby leading to a degeneracy between H_0 and emissivity. On the other hand, combining the dust time lags with near-IR interferometry allows measurement of direct distances to AGN (Hönig et al. 2014), which can be used to independently measure H_0 and self-consistently calibrate the AGN hot-dust standard candle.

4 SIMULATING THE VEILS TRANSIENT SURVEY FOR AGN

In this section, we will outline VEILS and quantify the expected constraints on cosmological models by using AGN dust lags as obtained in the course of the survey. As demonstrated, VEILS will allow us to observationally establish AGN dust lags as a new standardizable candle. With this new tool in hand, it will be possible to address tensions of low- and high-redshift constraints on cosmological parameters independently (e.g. Riess et al. 2016, and references therein). The survey simulations and strategies described in the following have been tested against observations and approximately reproduce the observed scatter of the lag–luminosity relation (see Appendix A).

4.1 Overview of VEILS

The VEILS is a new public *J*- and K_s-band survey on the 4-m VISTA telescope at ESO's Paranal Observatory (Chile). Rather than providing limits on total survey depths, the survey strategy emphasizes symbiosis between cadenced observations with per-epoch depths required by transient science cases (AGN and supernovae) and combined survey depths suitable for a range of galaxy evolution science cases.

VEILS is scheduled to run over 3 yr with approximately 6-month long observing seasons each year. We target 3 deg^2 regions in each of the Chandra Deep Field South, Elias South field, and XMM deep field for a total of 9 deg^2. The selected regions are simultaneously covered by the Dark Energy Survey (DES), which provides us with contemporaneous *griz* light curves, complementing the *J* and K_s light curves from VEILS. DES will observe each field about every 7 d while VEILS will repeatedly visit each field every 10–14 d. This will result in approximately 15 epochs per field per observing season or 45 epochs over 3 yr in total. As demonstrated below, these kind of multiband time-domain observations will allow for reconstructing enough AGN dust time lags to put competitive constraints on cosmological parameters. Table 1 summarizes cadence and per-epoch depths for each filter. These parameters will be used for the survey simulations below. It is possible that DES will finish

Table 1. Survey parameters used as input to the simulations.

Survey	Cadence (d)	Filter	5σ per-epoch depth (AB mag)
VEILS	14	K_s	22.5
		J	23.5
DES	7	z	24.0
		i	24.3
		r	24.1
		g	24.5

Note. The DES limits correspond to an analysis of the combined year 1–3 deep transient fields, which are also targeted by VEILS (M. Smith, private communication).

operations before the end of VEILS. In this case, we will complement the near-IR survey with optical observations to the same depth and similar cadence at the VLT Survey Telescope (VST), which is operated by ESO on the same site as VISTA.

4.2 Defining an AGN mock sample

VEILS will cover a total area of 9 deg^2 for which we have to estimate the number of type 1 (=unobscured) AGN that can be detected. In order to create a mock sample of AGN with realistic parameters, we took the redshift-dependent optical luminosity function of Palanque-Delabrouille et al. (2013) and estimated the number, luminosity distribution, and redshift distribution of all unobscured AGN within the survey area. After accounting for the 5σ detection limits of DES in *griz* (see Table 1), we are left with a sample of about 1350 type 1 AGN and we define these as our AGN mock sample. Note that since our sources are variable, the 5σ limits refer to the long-term mean magnitude.

4.3 Variability and survey simulations

We follow previous work in Hönig (2014) to characterize the variability in the AGN mock sample and simulate optical and infrared light curves. This involves modelling the AGN variability as a stochastic correlated autoregressive (CAR) process (e.g. Kelly, Bechtold & Siemiginowska 2009; Kelly et al. 2013). For all the AGN in our sample, we assigned black hole masses to the luminosities drawn from the luminosity functions by assuming an Eddington ratio log-normal distribution centred at $\log l_{Edd} = -1.2$ and a standard deviation of 0.3 dex (this covers Seyfert galaxies and quasars in the detectable luminosity range; see note at the end of this section). Kelly et al. (2013) show how the parameters of the CAR process correlate with observed AGN black hole masses and luminosities. We use these empirical relations, including their large scatters, to assign variability characteristics to the AGN mock sample. Based on these parameters, we simulate light curves for all of the bands and account for the observed dependence of variability amplitude on wavelength ('bluer when brighter' with amplitude $\propto \lambda^{-0.28}$; Meusinger, Hinze & de Hoon 2011).

The simulated AGN 'BBB' light curves are used as input to a dust radiative transfer model to simulate the response of the dust emission to the AGN variability. We parametrize the dust distribution in terms of an observationally motivated projected radial power law $\propto r^a$ (e.g. Kishimoto et al. 2009; Hönig & Kishimoto 2010; Kishimoto et al. 2011b) and an effective response amplitude w_{eff}, which sets the fraction of dust/infrared light that actually varies (Hönig & Kishimoto 2011). We assign random parameters from a range of $0.25 < w_{eff} < 0.85$ and $-2.5 < a < -0.5$ (a detailed

description of the process is available in the method section of Hönig et al. 2014, and references therein). In short, these parameters provide a realistic picture of how strongly the near-IR emission will react to the incident AGN variability and to what extent the variability will be smeared out.

After combining the AGN and dust light curves in each filter, we apply the VEILS and DES survey constraints listed in Table 1 to the light curves (see Section 4.1), and account for the noise characteristics in the DES and VEILS bands as well as some inhomogeneity in the observing cadence due to scheduling or bad observing conditions. In Fig. 1, we show simulated light curves and mock observations for six AGN from the mock sample. The coloured lines represent the input model light curves for different bands, while the data points reflect the 3-yr survey, including 6-month seasonal gaps, with a median distance between each epoch corresponding to the DES and VEILS cadence. As illustrated by these examples, the significance of detecting a lag between optical and IR emission depends on various factors such as variability characteristics, response/transfer function, and redshift (= rest-frame wavelength of the K_s band).

We note that the exact shape of the $\log l_{Edd}$ distribution does not affect the properties of the final AGN sample noticeably: in testing a log-uniform distribution with $-2 < \log l_{Edd} < -0.4$, we recovered the same redshift and luminosity distribution of those objects that are detectable within the DES survey constraints.

4.4 Recovering dust lags from the DES + VEILS light curves

With the mock survey observations in hand, we aim at recovering the dust lags as precisely as possible. The success rate mainly depends on the S/N of the observations, the cadence, and the fraction of dust emission varying in the K_s band, which is a mixture of an AGN-intrinsic property (see Section 4.3) and redshift.

The standard method to determine dust lags is to calculate the cross-correlation function (CCF) for a range of lags and determine the peak. However, this technique requires well-sampled light curves and good S/N ratios; otherwise the CCF will have low values, and it becomes difficult to distinguish between the true lag and spurious peaks. Also, this method is strongly affected by the window function of the observations (seasonal gaps, total survey coverage). Instead, we attempt to recover the time lags with a technique that maximizes the use of information within the light curves. For this, we make use of the fact that the dust light-curve $F_{dust}(t)$ is a rescaled, smeared-out and shifted version of the UV/optical light-curve $F_{BBB}(t)$, i.e.

$$F_{dust}(t) = \int F_{BBB}(t' - \tau) \cdot \Phi(t - t') \, dt', \qquad (4)$$

where τ is the lag between the hot-dust variability and the optical variability, and $\Phi(t)$ is the transfer function, which controls the smearing and rescaling. The key idea behind this approach is that dust reprocesses the UV-peaked BBB emission into infrared photons. This description resembles previous studies of broad emission line lags (e.g. Zu, Kochanek & Peterson 2011; Chelouche & Daniel 2012; Chelouche & Zucker 2013) with the extension that we do parametrize $\Phi(t)$ instead of assuming an ad hoc shape (see below). Moreover, as discussed in Hönig et al. (2014), we do not use the full dust and BBB light curves for lag recovery, but only the relative variability $(F(t) - \langle F(t) \rangle)/\langle F(t) \rangle$ about the mean $\langle F(t) \rangle$. This procedure better isolates the variability pattern and the effect of $\Phi(t)$.

A caveat in recovering the dust lags arises from the fact that the observed light curves are not continuous but contain gaps of varying lengths. In order to overcome this problem, we invoke the popular flux randomization/random subset selection (FR/RSS) method (Peterson et al. 1998). It uses the variability characteristics of the observed light curves (i.e. typical flux changes for given intervals) to interpolate regularly spaced random realizations of the light curves based on a Monte Carlo method. In principle, we could use the CAR process invoked to generate the mock light curves to interpolate the mock-observed light curves. This would involve fitting the observed power spectra with the CAR prescription and picking fluxes between observed epochs according to the fitted CAR parameters. However, in this case we would implicitly use our knowledge about the process that generated the variability to recover the light curves, which carries the risk that the errors on the final recovered lags would be underestimated. In addition, recent Kepler observations challenge the CAR process as the driver for accretion variability in AGN (Mushotzky et al. 2011), which is why a more data-driven approach to light-curve interpolation (such as FR/RSS) will introduce less model dependence for the real survey.

The scheme we follow to model the light curves and recover dust lags starts with determining $F_{BBB}(t)$. For that, we make use of the multiband coverage of the BBB emission in the DES *griz* filters and, for higher redshift sources, the VISTA *J* filter. Indeed, we cover the 0.3–0.9 μm rest-frame region with at least four filters in all of the targeted redshift range of $0 < z < 1.2$. In using information from at least four broad filters, we are also less sensitive to potential contamination by emission lines and their variability. In fact, given an object's redshift, it is possible to sub-select an optimal set of filters to minimize broad-line contamination. We resample observations in each band 20 times using the FR/RSS method, with the number of samples limited by computational resources. For each epoch observed by at least one of the *grizJ* bands, we determine the BBB continuum spectral slope via a power-law fit, determine the flux at a rest-frame wavelength of 550 nm, and assign errors according to the variation among the randomly resampled light curves. The result is a very high-quality light curve of the driver emission for the dust variability (see Fig. 2, blue data points).

In the next step, we recover the dust variability. For this, we start with the FR/RSS-resampled light curves in each of the *grizJ* bands. We then fit a power law to the resampled *grizJ* flux at each K_s-band epoch and extrapolate the power law to the K_s band. This provides us with the BBB contribution to the K_s band. We then subtract the BBB contribution from the observed K_s data and obtain a clean hot-dust light curve, which we will just refer to as the 'dust light curve' in the following. Recovered BBB and dust light curves for the six example objects in Fig. 1 are shown in Fig. 2.

Next, we take the recovered BBB light curve at 550 nm rest frame as input to fit equation (4), after subtracting and normalizing by the mean flux, and parametrize the transfer function $\Phi(t)$ in terms of a power-law flux decay in time. For broad lines, the adoption of a top-hat transfer function has become very common. However, there is strong evidence from IR interferometry as well as radiative transfer theory that, at least for the dust, a power-law shape is more appropriate (e.g. see Hönig & Kishimoto 2011; Hönig et al. 2014). Therefore, we fit for a parametrization of the transfer function

$$\Phi(t) = \Phi_0 \cdot (t/\tau + 1)^\alpha, \qquad (5)$$

where τ is the time lag, α is the power-law index of the brightness distribution, and Φ_0 is the normalization amplitude to obtain $\int_0^\infty \Phi(t) \, dt = 1$.
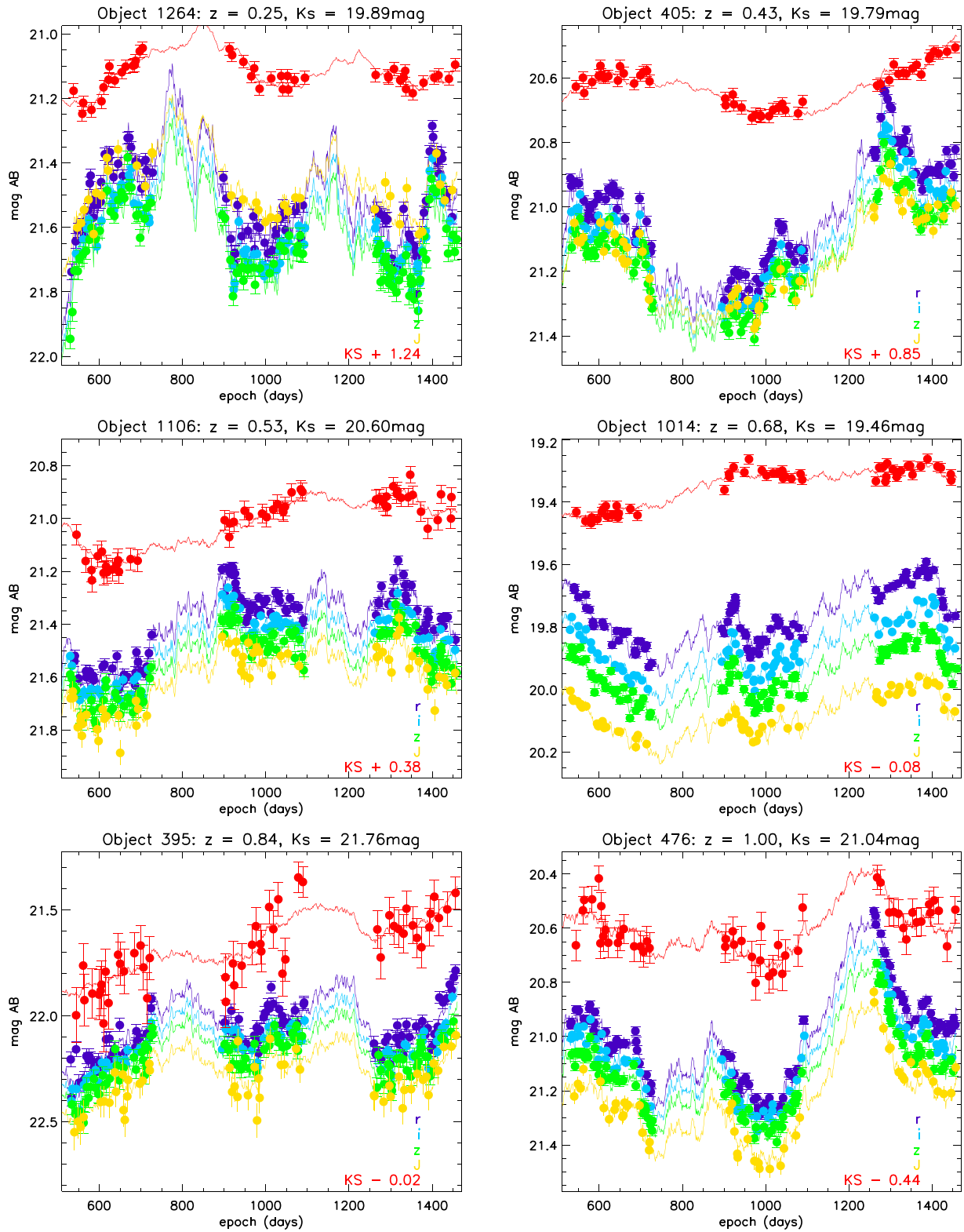
Figure 1. Simulated and mock-observed light curves for six objects in our mock AGN sample. The purple, blue, and green dotted lines represent the input AGN light curves in the DES *riz* bands while the yellow and red dotted lines are *J*- and K_s-band light curves in the VIRCAM bands (K_s is shown as the upper-most curve in each panel). The filled circles with error bars represent the 3-yr mock survey observations, which account for the limiting magnitudes in each band, the survey cadence, and the seasonal gaps. The K_s-band light curves are offset for illustration purposes and the offset is noted in each panel where applicable. The running numbers refer to the full type 1 AGN sample of 1350 objects.
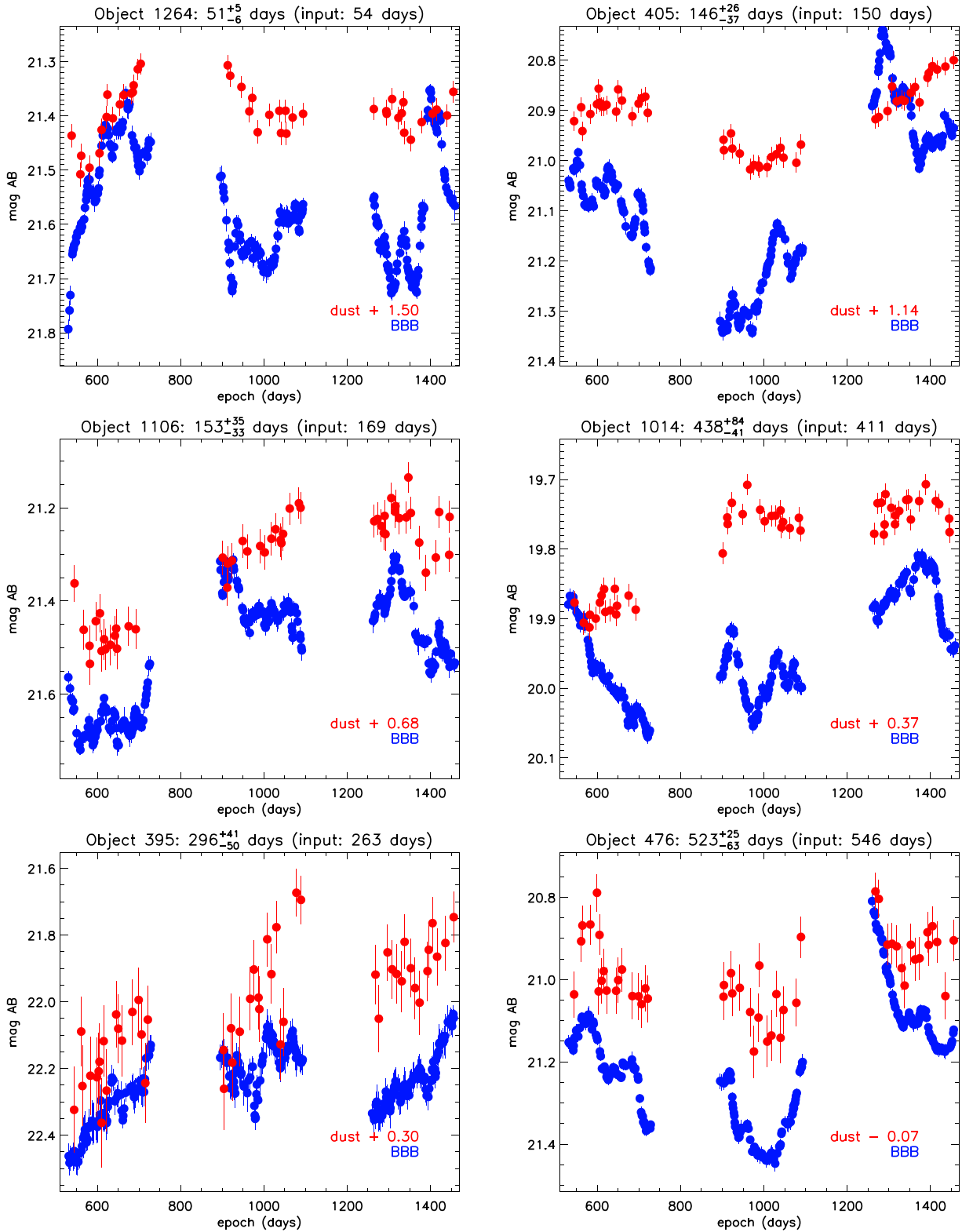
Figure 2. Dust time lag recovery for the six examples in Fig. 1. The blue/darker circles with error bars show the recovered BBB light curve at 0.55 μm rest-frame wavelength. The red/lighter data points correspond to the recovered hot-dust light curve in the observed K_s band after subtraction of the BBB component, with offsets indicated. As the redshift increases, the contribution of dust emission to the K_s band decreases but lags can still be recovered. The recovered lags (observer frame) with errors and input lags are indicated in the headline of each panel.
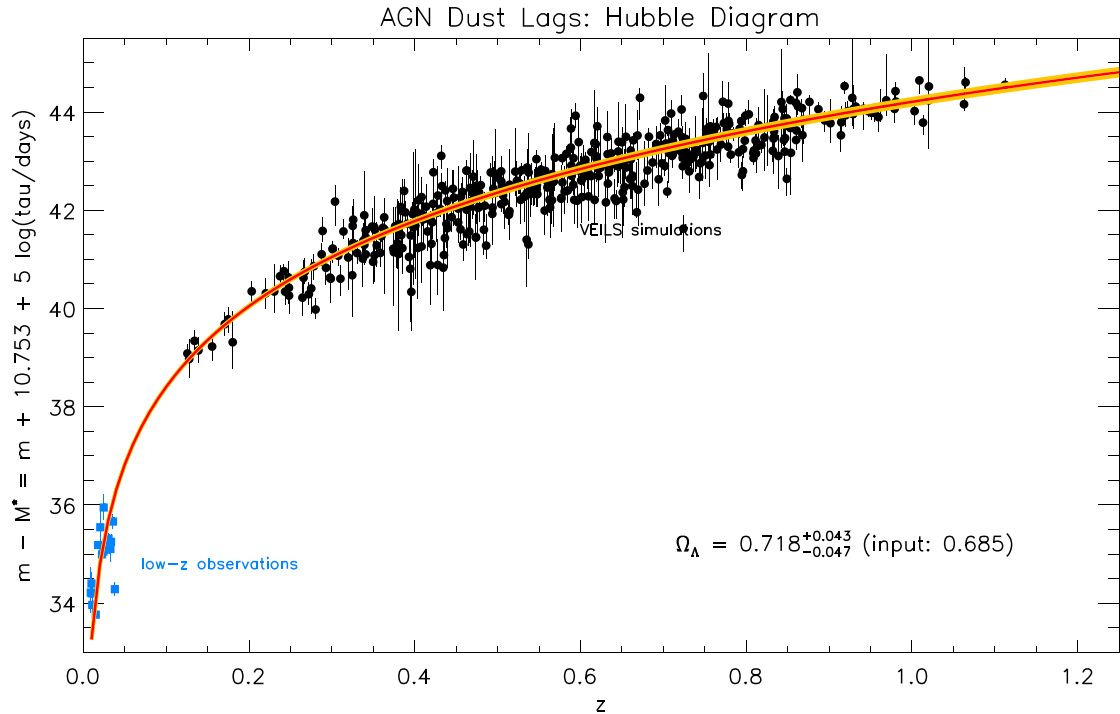
Figure 3. Hubble diagram based on the 437 AGN dust lags recovered in our VEILS simulations based on 3-yr light curves with about 15 observed epochs in the K_s band per 6-month observing season. The red line indicates the best-fitting ΛCDM cosmology with flat geometry and the orange lines represent the 68 per cent confidence region. The inferred dark energy density parameter is indicated. We also overplot the current low-z sample from literature (blue squared data points) to illustrate how they may be used to help determining the normalization of the Hubble function (see text for details).

The BBB light curve is FR/RSS-resampled and a time lag with uncertainty is inferred by fitting the resampled, shifted and normalized BBB light curve to the observed dust light curve via the power-law index of $\Phi(t)$, an offset of the mean magnitude, and a stretch factor, using the Levenberg–Marquardt algorithm implemented in *mpfit* (Markwardt 2009). For each resampled version, the χ^2 space is very uneven with several local minima. To distinguish the various minima objectively and without expectation bias, we redo the fitting for each of the resampled light curves 50 times by selecting random-uniform starting parameters. The most frequent τ (a 'dominant χ^2 minimum') is considered the best-fitting value for the particular BBB resample.

The fitting procedure is repeated for 40 random FR/RSS Monte Carlo-resampled versions of the BBB light curve. In this process, we also take into account the uncertainties in the recovered dust fluxes and the limited sampling of the dust light curve. Finally, we calculate a mean τ and 68 per cent confidence intervals from the distribution of fitted lag values in all FR/RSS samples. This recovered τ explicitly includes the effects from sparse and inhomogeneous sampling of the dust and BBB light curves.

5 RESULTS

5.1 Dust lag-recovery statistics

We applied our dust lag-recovery procedure to the 1350 type 1 AGN. Given the survey characteristics, we have about 15 K_s-band mock observations per annual observing season, adding up to a total of ~45 observations for each object over the 3-yr VEILS campaign. Out of the 1350 type 1 AGN, we recovered lags for 437 of the AGN, or 32 per cent. This number should be considered a conservative approach since we did not follow through with our lag-recovery

process if the recovered hot-dust emission has S/N <5 according to the K_s-band limit of 22.5 mag. We also did not attempt to recover a time lag if the expected lag was >730 d. This corresponds to a situation where the first observing season in the BBB light curve drives dust variability in the last observing season. However, some of the final fitted lags may be longer than 730 d because either the expected lag estimate was too short or the fitting procedure settled for a longer lag.

At magnitudes fainter than 22.5 mag, it becomes increasingly difficult to define a global minimum in χ^2 consistent among all resampled BBB light curves. Similarly, trying to recover longer lags will result in <15 observations to be used to fit the dust light curve. We will review if the number of recovered lags can be increased without compromising the quality of recovered lags once real data are available. For the purpose of this paper, the 437 recovered lags form the basis for constraining cosmological parameters.

5.2 Constraints on cosmology

In this section, we demonstrate the suitability of AGN to constrain cosmological parameters. The simulations of AGN light curves are based on a dark energy density $\Omega_\Lambda^{\text{in}} = 0.685$ and $w^{\text{in}} = -1$. These are the parameters we aim at recovering by using the distance moduli based on the recovered dust time lags.

5.2.1 Dark energy density Ω_Λ

In Fig. 3, we present a Hubble diagram for the 437 AGN with recovered dust time lags. The plot shows the distance modulus $m_V - M_V^*$, calculated from equation (3) for all objects, versus redshift z. In addition, we show the best-fitting Hubble function to the distance

Table 2. Comparison of constraints on Ω_Λ from different surveys.

Survey	Number of objects			Ω_Λ in ΛCDM		Reference
	All	$z > 0.3$	$z > 0.7$	stat.	stat. + syst.	
Union 2.1 type Ia supernovae	580	285	90	$0.723^{+0.022}_{-0.021}$	$0.705^{+0.043}_{-0.040}$	Suzuki et al. (2012)
JLA type Ia supernovae	740	270	108	0.711 ± 0.018	0.705 ± 0.034	Betoule et al. (2014)
VEILS AGN simulations	437	408	143	$0.718^{+0.043}_{-0.047}$		This work; input $\Omega_\Lambda = 0.685$

moduli based on a flat ΛCDM cosmology (i.e. no curvature and $w = -1$; see Section 3). The fit has two free parameters: (1) the dark energy density Ω_Λ, and (2) the normalization k_n of the AGN distance moduli. Both parameters were fitted jointly. When marginalizing over Ω_Λ, we obtain a normalization of $-2.5 \log k_n = (10.753 \pm 0.044)$ mag. It should be noted that sensitivity to cosmological model increases with redshift while the normalization is sensitive to lower redshift. Since both Ω_Λ and k_n are correlated, it is important that observation cover a range of redshifts to reduce the uncertainties in inferred parameters. In this work, we focus on the VEILS-only AGN with redshifts $z > 0.12$. Further high-quality low-redshift AGN dust time lags are available in literature and may be used as additional input once VEILS data are available (currently at least 20 objects; Suganuma et al. 2006; Koshida et al. 2014; Pozo Nuñez et al. 2014, 2015). These are shown in Fig. 3 for comparison.

From our simulated lag measurements, we are able to constrain the dark energy density $\Omega_\Lambda = 0.718^{+0.043}_{-0.047}$ after marginalizing over k_n. This implies that we recovered the simulation input dark energy density well within the 1σ confidence interval and with a precision of 6 per cent. We can compare these AGN-based constraints to current type Ia supernova samples. Suzuki et al. (2012) presented the Union 2.1 sample, which contains 580 supernovae (SNe). More recently, Betoule et al. (2014) compiled 740 type Ia SNe in the joint light-curve analysis (JLA). A comparison between both samples and the VEILS AGN simulation constraints on Ω_Λ is shown in Table 2. All three samples have comparable errors despite differences in sample sizes. The reason for this is the redshift distribution in the samples. The majority of AGN have redshift $z > 0.3$ while the supernovae are strongly biased towards lower redshifts. This makes AGN more sensitive to the changes in the Hubble function when invoking different cosmological parameters. On the other hand, the scatter of AGN around the mean function is higher, which compensates for the higher redshifts. In summary, the quality of recovered Ω_Λ demonstrates the potential of AGN dust lags as standard candles. It should be noted that the remaining intrinsic scatter in the recovered dust time lags and, in turn, distance moduli is moderate: In order to obtain a reduced $\chi_r^2 = 1$, we needed to add $\sigma_{int} = 0.19$ mag to each object.

5.2.2 The equation of state in wCDM cosmology

We further test what new information AGN will contribute to constraining non-standard wCDM cosmology. For that, we follow the same fitting procedure as in the previous sub-section, but leave w as a free parameter. In Fig. 4, we show the 68 per cent confidence interval on combined dark matter density Ω_m and w constraints for the simulated VEILS AGN. These are compared to a fit to the Union 2.1 SNe distance moduli from Suzuki et al. (2012).[2] The confidence regions are slightly inclined with respect to each other. Since the AGN are at higher redshifts, they are more sensitive to

---

[2] We note that the VEILS AGN simulations have been rescaled for this illustration, so that the input Ω_m matches the SNe best fit in this parameter.
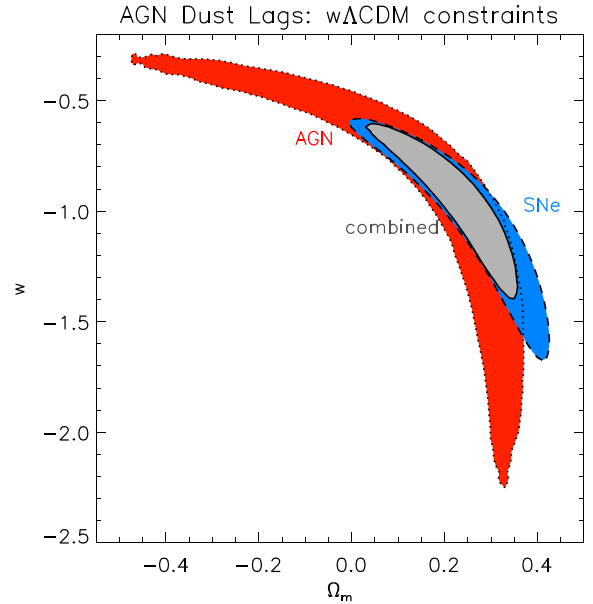
Figure 4. 68 per cent confidence regions for the w and Ω_m parameters in a flat $w\Lambda$CDM cosmological model. The red area with dotted boundary indicates constraints based on the VEILS AGN dust time lags only while the blue area with dashed boundary shows the SNe-only constraint based on the Union 2.1 sample. The grey area with solid boundary represents the joint 68 per cent confidence region.

w than current SN data. We also overplot the joint SNe + VEILS-AGN 68 per cent confidence region, which shrinks the combined uncertainty area.

When marginalizing over Ω_m, the quality in constraints on w are looser for the simulated VEILS AGN dust lags ($w = -1.00^{+0.52}_{-0.93}$) than for the Union 2.1 SNe (fit $w = -1.02^{+0.33}_{-0.40}$, including systematics). Improvements are seen when jointly analysing both local standard candles, which results in $w = -0.92^{+0.30}_{-0.36}$. This 10 per cent reduction in errors is primarily due to the redshift differences between the two object classes, even if the constraints from AGN are weaker than from SNe. However, the major step forward in constraining w involves the joint analysis of these confidence regions with the cosmic microwave background (CMB) and baryonic acoustic oscillations (BAO). The confidence regions of these cosmological probes are essentially perpendicular to the SNe and AGN dust lags.

6 DISCUSSION OF PRACTICAL CHALLENGES IN CARRYING OUT AN AGN DUST LAG SURVEY

6.1 AGN identification, selection, and redshifts

Using AGN dust lags in cosmology does not require a uniform or well-selected AGN sample. In fact, any AGN that shows sufficient

optical and near-IR variability to determine a time lag of the hot dust will suffice. Suitable AGN will be unobscured type 1 AGN with luminosities corresponding to time lags of order a few tens to several hundreds of days, given the flux limit of the survey and the redshift range limit implied by the K_s-band filter as the reddest observed waveband. The remaining challenge for such a survey in terms of defining a sample lies in identification of the AGN and obtaining their redshifts. VEILS will target three well-studied regions with a wealth of multiband information and catalogues. Given our magnitude limits, we expect that a large fraction/majority of the AGN have been pre-identified. Indeed, the OzDES spectroscopic survey (Yuan et al. 2015) already includes 1700 AGN in the 30 deg^2 DES deep fields, which partly overlap with our fields. Further spectroscopic follow-up may be necessary to classify previously unidentified AGN.

6.2 Host galaxy subtraction

The AGN-dust lag method presented here involves three observables: the time lag, the redshift, and the apparent magnitude of the AGN. We discussed the lag-recovery strategy (see Section 4.4) and spectroscopic redshifts (see previous section), but it is still necessary to recover the mean AGN magnitude from the underlying host galaxy. While this may be challenging for each individual epoch, our strategy is to combine images from all observed epochs to be able to use well-established host modelling and subtraction tools to disentangle AGN and galaxy on high-S/N multiband data (e.g. Peng et al. 2010). Indeed, given the simultaneous analysis/decomposition of spectroscopic data and DES + VEILS *grizJK*$_s$ six-band imaging data, we expect to be able to constrain the AGN magnitude to within a fraction of the uncertainty of the lags, which means that we do not expect our cosmological constraining power to be affected by host subtraction. With this multidimensional approach, we will also be able to address any potential extinction by adding an extinction component to the decomposition. It is worth mentioning that our simulations build upon the empirical lag–luminosity relation that was obtained under much less ideal conditions than the ones in VEILS: the bulk of the currently available data originates from the 2 m MAGNUM telescope with much lower sensitivity, less angular resolution, and only one optical band (see Koshida et al. 2014, and references therein). We will quantitatively assess the influence of the host galaxies in VEILS in a future paper once real data are available. However, it is important to note that a systematic bias in any such host-AGN decomposition technique would not affect the constraints on cosmology since this would be absorbed by the normalization k_n of the whole sample.

A second possibility is using the variable component in each of the *grizJ* bands as the BBB reference. This circumvents host decomposition and extinction effects, but ignores any non-variable part of the BBB, which may still contribute to dust heating and influence the size of the sublimation radius. If this non-variable fraction is small, it would result in a systematic bias, which will be implicitly compensated for in the normalization of the Hubble function. On the other hand, if this fraction is luminosity dependent, it would skew the Hubble function. In case of very strong host contamination, the variability of the AGN will be significantly diluted, which increases the measurement errors. We propose to put this to a test with real data, in particular because it has the potential to circumvent any systematic uncertainty from the absolute flux calibration of the images.
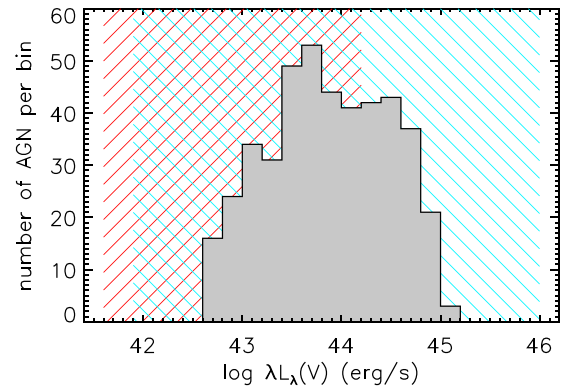

Figure 5. Distribution of *V*-band luminosities of those 437 AGN for which dust time lags were recovered. The red up-hatched area shows the luminosity range covered by low-*z* dust reverberation mapping while the blue down-hatched area delineates the range covered by near-IR interferometry.

6.3 Evolution of the lag–luminosity relation

One unknown in the use of AGN dust time lags as standardizable candles is a potential redshift evolution of the lag–luminosity relation. This evolution may originate from two sources: (1) a change in metallicity, and (2) non-linearity in luminosity. In Section 2, we argue that metallicity is probably a minor concern given that we observe the hottest dust with emissivity close to a blackbody. The major risk of evolution with luminosity comes into play if we reach beyond the luminosity range covered by current low-redshift lag–luminosity studies. Therefore, we compare the range of luminosities for which we recover dust lags in VEILS to the range established by current low-redshift observations. The 17 reverberation-mapped objects in Koshida et al. (2014) span a range of *V*-band luminosities of about 10^{42} erg s^{-1} < $\lambda L_\lambda(V)$ < 10^{44} erg s^{-1}. In addition, near-IR interferometry size measurements at low redshift (e.g. Kishimoto et al. 2009, 2011a, 2013) cover approximately 10^{42} erg s^{-1} < $\lambda L_\lambda(V)$ < 10^{46} erg s^{-1}.[3] In Fig. 5, we compare these ranges with a histogram of *V*-band luminosities for those 437 VEILS AGN where we recovered dust time lags. The figure shows that VEILS AGN used for cosmology will cover the same range in luminosity as current low-redshift samples based on which the lag–luminosity relation has been established. This mitigates the risk of luminosity evolution. Nevertheless, we plan to split the observed AGN into sub-samples of different luminosities or metallicities to test if the inferred cosmological constraints differ systematically.

7 CONCLUSION AND LEGACY VALUE TO FUTURE HIGH-REDSHIFT AGN COSMOLOGY STUDIES

In this paper, we introduce a new survey that will observationally establish AGN dust time lags as cosmological standardizable candles. We will utilize time-sampled near-IR *J*- and K_s-band data of well-studied extragalactic survey fields and combine them with simultaneous multiband optical data to determine dust time lags of

---

[3] When combining *K*-band time lags and interferometry, there is a well-known offset in normalization (e.g. Kishimoto et al. 2007, 2009; Koshida et al. 2014). This offset is caused by the underlying dust/brightness distribution and the related sensitivity of the two methods to spatially extended emission (e.g. Hönig & Kishimoto 2011). Modelling the reverberation transfer function allows for compensation of this effect (Hönig et al. 2014).

several hundred unobscured AGN. Here, we simulate the survey and evaluate its power in constraining cosmological parameters. We conclude the following:

(i) The new VEILS public survey with VISTA VIRCAM has the capability to fully establish AGN dust time lags as a new standard candle for cosmology. It is complementary to type Ia supernovae and can assess hidden systematics in the same redshift range targeted by current SNe surveys (e.g. DES).

(ii) We showed that the constraints on Ω_Λ obtained from the AGN dust lags will be competitive with type Ia supernovae while improvements in w constraints will require a joint AGN + SNe analysis. Indeed, by combining both standard candles, we will be able to improve current Ω_Λ constraints by ∼20 per cent and by ∼10 per cent for w. This opens prospects to further narrow down any potential differences between low-redshift and higher redshift cosmological probes (e.g. BAO and CMB).

(iii) Future efforts in cosmology will focus on higher redshift probes to constrain w_a and w_0. The time lag between optical continuum emission in AGN and their broad emission lines will be a key standard candle to reach higher redshifts of $z \sim 4$ (e.g. Watson et al. 2011; Czerny et al. 2013; King et al. 2014). Since the AGN dust time lags probe exactly the same object class (=unobscured AGN), the dust time lags can provide the low-redshift normalization for the high-redshift studies. Many of the VEILS AGN will be monitored with OzDES spectroscopically, which allows for cross-calibration between dust lags and BLR lags and provide the springboard to high redshifts.

One of the most substantial advancements will be an immediate growth in the number of low-redshift standard candles when combining SNe with AGN. For that we will need a cross-calibration reference. Li et al. (2011) find an SN Ia rate of 0.54 ± 0.12 per century for a Milky Way-type galaxy at $z = 0$. Assuming that the Milky Way mass, luminosity, and Hubble type is typical of a Seyfert AGN-hosting galaxy, and considering an increase of the SNe Ia rate by at least a factor of 3 to redshift 0.5 (see also Li et al. 2011), we expect that about 5–15 of the AGN hosts with an established dust lag in VEILS will display an SN Ia during the lifetime of the survey. These galaxies will serve as the basis to merge the low-redshift standard candles.

REFERENCES

Barvainis R., 1987, ApJ, 320, 537
Betoule M., Kessler R., Guy J. et al., 2014, A&A, 568, 22
Chelouche D., Daniel E., 2012, ApJ, 747, 62
Chelouche D., Zucker S., 2013, ApJ, 769, 124
Czerny B., Hryniewicz K., Maity I., Schwarzenberg-Czerny A., Życki P. T., Bilicki M., 2013, A&A, 556, 97
Elvis M., Karovska M., 2002, ApJ, 581, L67
Haas M., Chini R., Ramolla M., Pozo Nuñez F., Westhues C., Watermann R., Hoffmeister V., Murphy M., 2011, A&A, 535, 73

Hönig S. F., Kishimoto M., 2010, A&A, 523, 27
Hönig S. F., Kishimoto M., 2011, A&A, 534, 121
Hönig S. F., Watson D., Kishimoto M., Hjorth J., 2014, Nature, 515, 528
Hönig S. F., ApJ, 784, L4
Horne K., Korista K. T., Goad M. G., 2003, MNRAS, 339, 367
Keel W. C., Lintott C. J., Schawinski K. et al., 2012a, AJ, 144, 66
Keel W. C., Chojnowski S. D., Bennert V. N. et al., 2012b, MNRAS, 420, 878
Kelly B. C., Bechtold J., Siemiginowska A., 2009, ApJ, 698, 895
Kelly B. C., Treu T., Malkan M., Pancoast A., Woo J.-H., 2013, ApJ, 779, 187
King A. L., Davis T. M., Denney K. D., Vestergaard M., Watson D., 2014, MNRAS, 441, 3454
King A. L., Martini P., Davis T. M. et al., 2015, MNRAS, 453, 1701
Kishimoto M., Hönig S. F., Beckert T., Weigelt G., 2007, A&A, 476, 713
Kishimoto M., Hönig S. F., Tristram K. R. W., Weigelt G., 2009a, A&A, 493, L57
Kishimoto M., Hönig S. F., Antonucci R., Kotani T., Barvainis R., Tristram K. R. W., Weigelt G., 2009b, A&A, 507, L57
Kishimoto M., Hönig S. F., Antonucci R., Barvainis R., Kotani T., Tristram K. R. W., Weigelt G., Levin K., 2011a, A&A, 527, 121
Kishimoto M., Hönig S. F., Antonucci R., Millour F., Tristram K. R. W., Weigelt G., 2011b, A&A, 536, 78
Kishimoto M., Hönig S. F., Antonucci R. et al., 2013, ApJ, 775, L36
Koshida S., Minezaki T., Yoshii Y. et al., 2014, ApJ, 788, 159
Li W., Chornock R., Leaman J., Filippenko A. V., Poznanski D., Wang X., Ganeshalingam M., Mannucci F., 2011, MNRAS, 412, 1473
Lira P., Arévalo P., Uttley P., McHardy I. M., Breedt E., 2011, MNRAS, 415, 1290
Markwardt C. B., 2009, in Bohlender D. A., Durand D., Dowler P., eds, ASP Conf. Ser. Vol. 411, Astronomical Data Analysis Software and Systems XVIII. Astron. Soc. Pac., San Francisco, p. 251
Meusinger H., Hinze A., de Hoon A., 2011, A&A, 525, 37
Mushotzky R. F., Edelson R., Baumgartner W., Gandhi P., 2011, ApJ, 743, L12
Oknyanskij V. L., Horne K., 2001, ASPC, 224, 149
Oknyanskij V. L., Lyuty V. M., Taranova O. G., Shenavrin V. I., 1999, Astron. Lett., 25, 483
Palanque-Delabrouille N., Yèche C., Borde A. et al., 2013, A&A, 559, 85
Peng C. Y., Ho L. C., Impey C. D., Rix H.-W., 2010, AJ, 139, 2097
Peterson B. M., Wanders I., Horne K. et al., 1998, PASP, 110, 660
Phinney E. S., 1989, in Duschl W., Meyer F. & Frank J., eds, NATO Advanced Science Institutes (ASI) Series C, Vol. 290, Theory of Accretion Disks. Kluwer, Dordrecht, p. 457
Pozo Nuñez F., Haas M., Chini R. et al., 2014, A&A, 561, L8
Pozo Nuñez F., Ramolla M., Westhues C. et al., 2015, A&A, 576, A73
Riess A. G., Macri L. M., Hoffmann S. L. et al., 2016, ApJ, 826, 56
Suganuma M., Yoshii Y., Kobayashi Y., Minezaki T., Enya K. et al., 2006, ApJ, 639, 46
Suzuki N., Rubin D., Lidman C. et al., 2012, ApJ, 746, 85
Watson D., Denney K. D., Versergaard M., Davis T. M., 2011, ApJ, 740, L49
Yoshii Y., Kobayashi Y., Minezaki T., Koshida S., Peterson B. A., 2014, ApJ, 784, L11
Yuan F., Lidman C., Davis T. M., Childress M., Abdalla F. B. et al., 2015, MNRAS, 452, 3047
Zu Y., Kochanek C. S., Peterson B. M., 2011, ApJ, 735, 80

APPENDIX A: COMPARISON OF SIMULATED LAG–LUMINOSITY RELATION TO OBSERVATIONS

One goal of this paper is to provide simulations that reflect the observed dust lag–luminosity relation as close as possible to get a realistic estimate of how well cosmological parameters can be constrained. As a sanity check, we test if the scatter in the simulated τ–L relation is comparable to the real observed one, after processing
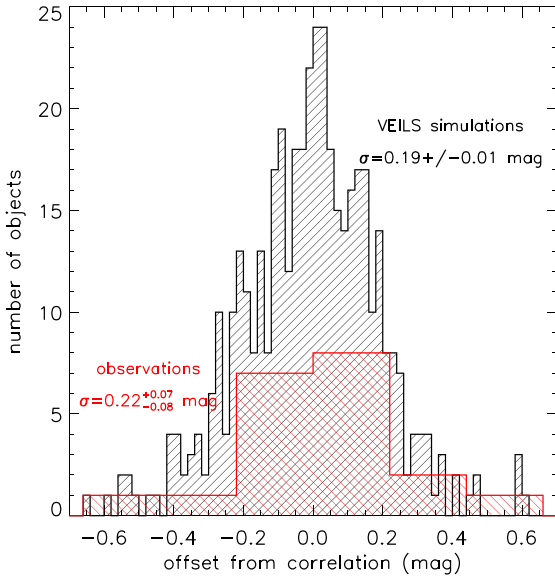
Figure A1. Distribution of inferred time lags from the simulations (black upward-hatched) and observed AGN (red downward-hatched), respectively, around the best-fitting lag–luminosity relation. The offsets are expressed in magnitudes as $2.5\log\tau - 2.5\log\tau_{\mathrm{pred}}$. 68 per cent confidence intervals are noted for both observed and simulated samples, with the uncertainties inferred from bootstrapping and accounting for the limited number of objects in each sample.

the mock light curves through our lag-recovery pipeline. In the following, L will be expressed as absolute magnitude M_V, which is ultimately used in the distance modulus.

We collect K-band lags and absolute V-band magnitudes M_V^{obs} of 20 AGN from the literature (Lira et al. 2011; Koshida et al. 2014; Pozo Nuñez et al. 2014, 2015). These are used as a comparison sample to our simulations. We then fit the inferred time lags from

the mock observations to the absolute magnitudes in the mock observations $M_V^{\mathrm{sim}} = m_V^{\mathrm{sim}} - 5\log D_{\mathrm{L}}/10\,\mathrm{pc}$, where m_V^{sim} is the mean apparent V-band magnitude of the AGN inferred from the multiband mock light curves. The luminosity distance D_{L} is calculated from the input redshift given input cosmological parameters. In order to make a comparison to observations, we treat M_V as the independent variable, predict the time lags τ_{pred} by fitting the M_V–τ relation, and plot the resulting offset of each data point from the best-fitting relation in histograms, for observations and simulations, respectively. These histograms are shown in Fig. A1 and the widths containing 68 per cent of the objects are noted. The error on these standard widths has been inferred from bootstrapping the samples to account for the finite number of observed sources in both observations and simulations.

The offsets are shown in magnitudes as $2.5\log\tau$–$2.5\log\tau_{\mathrm{pred}}$ to allow for a direct comparison with the observational uncertainties as well as the distribution in distance moduli. The observed and simulation-recovered lag–luminosity relations are consistent within error bars, with a nominally slightly narrower relations for the simulation-recovered lags. Indeed, it is entirely possible that the slightly narrower distribution in the simulations is driven by the better constraint on the AGN apparent magnitude given that at least four bands have been used to infer m_V instead of typically just one band in literature (with the exception of Lira et al. 2011). The consistent, and arguably superior, method to determine the time lags, which includes the information from the observed transfer function, may have also improved the scatter in the lags recovered from the simulations. In summary, we conclude that the simulations are properly reflecting the state of the art in dust time lag observations.

This paper has been typeset from a TₑX/LATₑX file prepared by the author.